Electronic Structure and Spectroscopic Studies of D_{3d}-$C_{60}Cl_{30}$, a Chlorofullerene with a [18]Trannulene Ring, and Its Relation to Other [18]Trannulenes

Alexey A. Popov,* Vladimir M. Senyavin, and Sergey I. Troyanov

Chemistry Department, Moscow State University, Moscow 119992 Russia

Received: January 24, 2006; In Final Form: March 25, 2006

Detailed spectroscopic characterization of D_{3d}-$C_{60}Cl_{30}$, including IR, Raman, UV−vis absorption, and fluorescence spectra, is presented for the first time. Assignment of the vibrational spectra is proposed on the basis of density functional theory computations. Electronic structure and excitations of $C_{60}Cl_{30}$ and other [18]trannulenes are studied theoretically with the use of time-dependent density functional theory and time-dependent Hartree−Fock approximation. Assignment of the low-energy part of electronic spectra of C_{60}-based [18]trannulenes is given and importance of the interactions between trannulene moiety and remaining π-subsystems in these molecules is established.

Introduction

Recently proposed chlorination of the fullerenes with metal chlorides resulted in isolation of several new chlorofullerenes[1,2] including particularly stable $C_{60}Cl_{30}$ with D_{3d} molecular symmetry.[3] Carbon cage of this molecule has a very specific drum-shaped structure with two isolated benzene rings on the poles and aromatic [18] trans annulene (also called trannulene) belt at the equator (Figure 1a). Other examples of [18]trannulenes are known in the fullerene chemistry, namely, the class of $C_{60}F_{15}R_3$-based derivatives[4,5] (Figure 1b) and recently synthesized $C_{60}R_6$[6] (Figure 1c) (R is a malonate group in both cases). These compounds were reported to have an emerald-green color in solution and significant absorption in the visible ($C_{60}F_{15}R_3$) or near-IR ($C_{60}R_6$) ranges, features not common for the fullerene derivatives and thus attributed to the presence of [18]trannulene rings.[4−7] A strong blue shift of the absorption bands in fluorofullerene trannulene compared to $C_{60}R_6$ was attributed to the influence of 15 fluorine atoms,[7] whose electron-withdrawing action is also manifested in a 0.5 V anodic shift of the first reduction potential versus $C_{60}^{0/-}$ pair.[8,9] Recently, photophysics of a series of dyads based on $C_{60}F_{15}R_3$ with photoactive substituents in malonate units was studied,[8,9] and intramolecular charge or energy-transfer relaxation pathways were documented depending on the substituent nature.[9] Despite increasing interest to fullerene-based trannulenes,[7] their electronic properties are not well understood yet.

$C_{60}Cl_{30}$ is, strictly speaking, the only "pure" trannulene, since [18]trannulene moieties in $C_{60}F_{15}R_3$ and $C_{60}R_6$ are partially conjugated with one and two triphenylene fragments, respectively. It is interesting how complete isolation of its aromatic subunits as well as collective action of 30 Cl atoms attached to the carbon cage in close proximity of [18]trannulene moiety affects the electronic properties of the molecule. In this work, we present first detailed spectroscopic studies of $C_{60}Cl_{30}$ supplemented with DFT quantum-chemical calculations and compare the electronic structure of this chlorofullerene to other fullerene-based [18]trannulenes.

* Author to whom correspondence should be addressed. E-mail: popov@phys.chem.msu.ru.

Experimental Section

$C_{60}Cl_{30}$ was synthesized as described elsewhere.[1−3] Electron absorption spectra were measured on a Specord-200 (Analytik Jena) spectrophotometer. Quartz cells with 1-cm optical path were used except for the measurements of *n*-hexane solution in the visible range that required 5-cm cell because of the low solubility of $C_{60}Cl_{30}$ in this solvent. The errors in extinction coefficient are estimated as 10−20%. Fluorescence emission spectra were measured on a Fluorat-2 Panorama (Lumex) spectrometer. IR spectra were measured on a Equinox 55 FT-IR (Bruker) spectrometer. Samples were pressed pellets of either pure $C_{60}Cl_{30}$ or $C_{60}Cl_{30}$ diluted with KBr. FT-Raman spectra were obtained with FRA 106 Raman module attached to Equinox 55 (excitation with 1064-nm line of Nd:YAG laser, resolution 2 cm^{-1}, 6000 scans).

Theoretical Methods

Geometry optimization and vibrational and time-dependent (TD) DFT calculations were performed with the PRIRODA package[10,11] using PBE functional[12] and implemented TZ2P-quality basis set. The quantum-chemical code employed expansion of the electron density in an auxiliary basis set to accelerate evaluation of the Coulomb and exchange-correlation terms,[11] also known as resolution-of-the-identity approximation. Raman intensities were computed numerically at the PBE/6-31G level using PC GAMESS.[13] For a better correspondence of experimental and computed vibrational spectra, DFT force field of $C_{60}Cl_{30}$ was scaled in the framework of inverse problem solution (see Supporting Information for details of the procedure). Additional TD-DFT as well as TD-HF and CIS computations were performed in 6-31G* basis with the use of PC GAMESS. Visualization of molecular orbitals was done with ChemCraft program (http://www.chemcraftprog.com).

Results and Discussion

Vibrational Spectra. Vibrational representation of D_{3d}-$C_{60}Cl_{30}$ spans into

$$\Gamma_{vib}(D_{3d}\text{-}C_{60}Cl_{30}) = 24A_{1g}(\text{Ram}) + 20A_{2g} + 44E_g(\text{Ram}) + 21A_{1u} + 23A_{2u}(\text{IR}) + 44E_u(\text{IR})$$

10.1021/jp060522m CCC: $33.50
Published on Web 05/23/2006

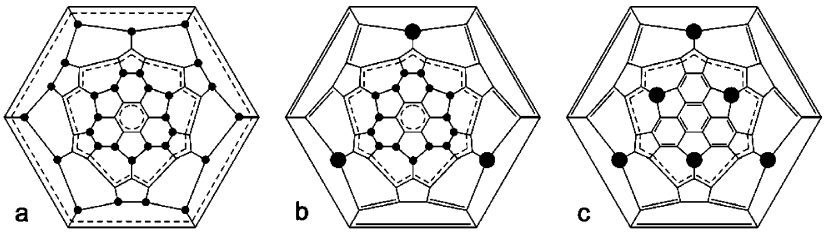

Figure 1. Schlegel diagrams of $C_{60}Cl_{30}$ (a), $C_{60}F_{15}R_3$ (b), and $C_{60}R_6$ (c). Small circles correspond to Cl or F atoms, and large circles correspond to malonate groups.

TABLE 1: Computed (Scaled DFT) and Experimental Frequencies (cm^{-1}) and Relative Intensities[a] of $C_{60}Cl_{30}$

sym	calc.	*I* (%)	exptl		sym	calc.	*I* (%)	exptl		sym	calc.	I (%)	exptl	
							Raman Modes							
A_{1g}	106.3	7.20	109	w	E_g	103.5	0.30			E_g	703.3	3.0		
A_{1g}	132.4	0.28			E_g	108.3	19.21	120	w	E_g	764.1	6.8	757	w
A_{1g}	168.6	8.61			E_g	119.6	9.66	134	w	E_g	812.8	22.1	816	w
A_{1g}	203.6	14.12	202	m	E_g	133.7	27.43	141	s	E_g	843.6	12.6		
A_{1g}	209.1	4.10			E_g	140.9	55.42	145	s	E_g	861.0	8.7		
A_{1g}	229.5	20.67	233	m	E_g	163.6	51.90	165	s	E_g	877.9	21.6	885	w
A_{1g}	260.5	66.41	266	s	E_g	178.3	5.48			E_g	900.5	0.8		
A_{1g}	297.2	3.84	304	w	E_g	198.1	1.79			E_g	921.5	13.8	929	w
A_{1g}	389.3	4.68	385	w	E_g	205.3	0.29			E_g	966.4	5.6		
A_{1g}	522.4	7.37	519	w	E_g	212.0	0.53			E_g	975.5	1.7		
A_{1g}	550.1	0.61			E_g	225.2	2.93			E_g	1040.0	9.7	1037	w
A_{1g}	657.7	0.11			E_g	231.3	10.47			E_g	1106.7	2.4	1103	w
A_{1g}	708.1	0.66			E_g	289.7	0.07			E_g	1148.9	16.6	1138	w
A_{1g}	743.8	1.64			E_g	304.9	0.05			E_g	1174.3	2.7		
A_{1g}	788.0	100.00	785	m	E_g	402.0	2.86	396	w	E_g	1227.8	0.5		
A_{1g}	830.4	7.28			E_g	430.2	4.39	428	w	E_g	1378.2	12.5	1380	m
A_{1g}	943.4	5.12			E_g	465.6	0.04			E_g	1441.2	11.1	1444	m
A_{1g}	987.2	16.04			E_g	484.0	0.17			E_g	1499.1	1.0		
A_{1g}	1031.8	6.56			E_g	525.4	5.91	519	w	E_g	1522.8	93.7	1506	vs
A_{1g}	1160.1	0.30			E_g	571.4	4.54			E_g	1658.8	3.6		
A_{1g}	1378.5	9.99	1380	m	E_g	604.7	1.96							
A_{1g}	1472.2	8.95			E_g	618.1	8.25	615	w					
A_{1g}	1482.0	37.55	1480	sh	E_g	654.3	3.70							
A_{1g}	1605.1	1.76	1616	w	E_g	697.7	8.36	697	w					
							IR Modes							
A_{2u}	110.0	0.75	110	w	E_u	97.3	0.01			E_u	661.4	0.00		
A_{2u}	128.6	0.05	128	vw	E_u	101.9	0.04			E_u	691.9	1.03	694	w
A_{2u}	201.4	1.47	201	w	E_u	117.2	0.03	117	vw	E_u	743.6	12.24	738	m
A_{2u}	202.1	0.01			E_u	130.7	0.08	128	vw	E_u	780.0	71.55	775	s
A_{2u}	222.9	0.06	224	vw	E_u	141.7	0.37	140	vw	E_u	816.3	100.00	823	vs
A_{2u}	229.0	1.15	234	w	E_u	175.4	0.00			E_u	846.8	7.75		
A_{2u}	264.8	0.12	265	vw	E_u	188.0	0.23	186	vw	E_u	871.5	6.92	869	w
A_{2u}	382.8	3.35	379	w	E_u	199.7	0.09			E_u	892.2	38.78	895	s
A_{2u}	441.2	2.60	439	m	E_u	210.2	0.00	211	vw	E_u	921.0	66.59	918	vs
A_{2u}	456.0	18.10	450	m	E_u	219.6	0.00	220	vw	E_u	946.5	2.09	943	vw
A_{2u}	652.0	0.82	657	w	E_u	247.4	0.12	246, 249	vw	E_u	982.7	24.91	993	m
A_{2u}	687.0	8.75	682	w	E_u	267.3	0.05	270	vw	E_u	1031.9	0.19		
A_{2u}	739.0	4.49	730	m	E_u	286.2	0.22	285	vw	E_u	1114.6	0.27	1114	vw
A_{2u}	778.3	6.09			E_u	312.7	0.23	313	vw	E_u	1158.7	1.77	1149	vw
A_{2u}	846.6	29.55	854	s	E_u	389.8	10.74	384	m	E_u	1173.8	0.80	1168	vw
A_{2u}	904.2	52.41	903	vs	E_u	445.1	1.28	439	m	E_u	1229.8	0.00		
A_{2u}	967.6	0.18	958	w	E_u	475.4	7.23	471	m	E_u	1447.5	15.38	1447	m
A_{2u}	989.2	0.63			E_u	480.6	10.66	479	m	E_u	1475.4	15.02	1478	w
A_{2u}	1083.6	0.10			E_u	529.4	0.04	526	w	E_u	1499.4	1.23	1517	vw
A_{2u}	1154.8	1.81	1149	vw	E_u	566.4	0.27	567	vw	E_u	1591.7	4.04	1614	vw
A_{2u}	1378.1	0.01	1389	vw	E_u	621.6	1.05	622	w	E_u	1658.6	0.05		
A_{2u}	1422.0	0.00			E_u	631.3	0.18	631	vw					
A_{2u}	1471.5	0.00			E_u	642.5	0.13	645	vw					

[a] Computed intensities are in % with respect to the most intense band, and experimental intensities are vs, very strong; s, strong; m, medium; w, weak; vw, very weak.

symmetry types; of these, 67 modes of A_{2u} and E_u symmetry are expected in the infrared spectra, and 68 modes of A_{1g} and E_g symmetry are Raman-active. From these modes, 49 IR and 31 Raman modes were determined in the corresponding experimental spectra (Table 1). In line with our previous work on chlorofullerenes,[14,15] DFT was found to underestimate C−Cl stretching and bending force constants. Therefore, DFT force field of the molecule was scaled with the use of scaling factors initially transferred from $C_{60}Cl_{24}$[14] and then adjusted in the framework of inverse problem solution (details of the procedure as well as a compete list of computed frequencies and potential energy distribution (PED) analysis of the normal modes can be

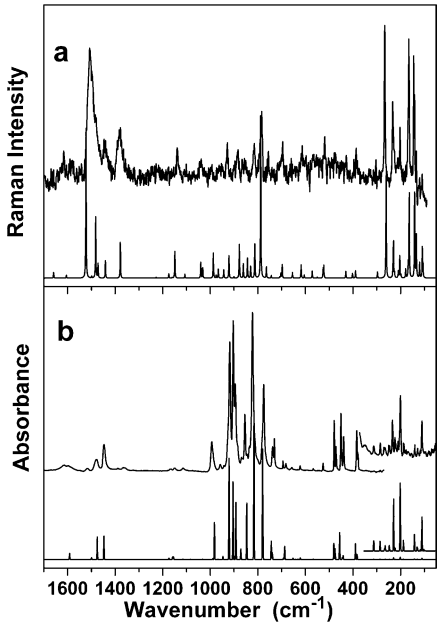

Figure 2. Experimental (upper curves) and scaled DFT (lower curves) spectra of $C_{60}Cl_{30}$: (a) Raman spectra, (b) IR spectra.

found in the Supporting Information). The procedure resulted in good agreement between computed and experimental spectra as shown in Figure 2 and enabled us to propose complete assignment of IR and Raman spectra of $C_{60}Cl_{30}$.

According to PED analysis, vibrations of $C_{60}Cl_{30}$ molecule below 300 cm^{-1} involve predominantly chlorine atom motions, while carbon contributions are less than 10−20%. This range exhibits many strong Raman and weak IR lines which can be described as bending C−Cl modes with admixture of radial cage deformations. The only exception is the strongest Raman line at 266 cm^{-1} which corresponds to the breathing mode of the carbon cage with only 13% of C−Cl bending.

Stretching vibrations of 30 C−Cl bonds formally constitute $3A_{1g} + 2A_{2g} + 5E_g + 2A_{1u} + 3A_{2u} + 5E_u$ normal modes, but actually C−Cl stretchings are inevitably mixed with CC(Cl)C deformations and C(Cl)−C(Cl) stretchings. Thus, q(C−Cl) contributions rarely exceed 40% for any mode and are scattered in the 300−900 cm^{-1} range. For instance, leading terms in PED for strong IR bands at 700−900 cm^{-1} are 30−40% C−Cl, 20−30% CC(Cl)C, and 10−15% CCCl.

Vibrations of $C_{60}Cl_{30}$ carbon cage may be best understood if the latter is treated as comprising rather rigid aromatic fragments (trannulene and benzene rings) imposed into the matrix of comparably long and flexible C−C bonds of C(sp^2)−C(Cl) and C(Cl)−C(Cl) types.[2,3] Thus, vibrations of aromatic subsystems are almost independent, and even a few modes caused by their "external" degrees of freedom can be established. For instance, translations of benzene rings (along C_3 axis, A_{2u}) and trannulene (perpendicular to C_3 axis, E_u) appear in the IR spectra at 379 cm^{-1} (w) and 383 cm^{-1} (m), respectively. Likewise, a weak Raman line at 385 cm^{-1} is also due to translations of benzene rings along the C_3 axis; this time, two rings move in the opposite directions, and the mode symmetry is A_{1g}. Specific "squashing" modes of the trannulene moiety occur around 430 cm^{-1}: a weak Raman line at 428 cm^{-1} corresponds to E_g-symmetric "ellipsoid" deformation of a nearly round trannulene ring (in hypothetical [18]trannulene $C_{18}H_{18}$ analogous mode is computed at 63 cm^{-1}), while A_{2u} "triangular" deformation of the moiety is responsible for the medium IR absorption at 439 cm^{-1} (analogous A_{1u} deformation is computed at 436 cm^{-1}, and these two modes

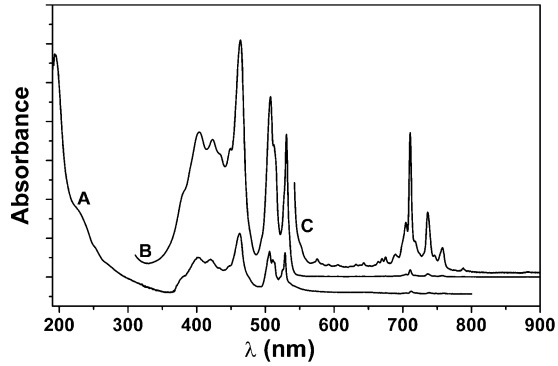

Figure 3. Room-temperature UV−vis absorption spectra of $C_{60}Cl_{30}$: (A) in *n*-hexane; (B) in toluene; (C) in toluene × 20.

correspond to the 2-fold degenerate vibration in $C_{18}H_{18}$ at 173 cm^{-1}). Totally symmetric breathing mode of the trannulene ring appears as a medium Raman line at 519 cm^{-1}.

Carbon−carbon stretching vibrations of benzene rings and trannulene moiety occur in the same frequency range, and the former are almost hidden behind much more intense trannulene bands. The latter are responsible for medium IR absorptions at 1447 and 1478 cm^{-1}, medium Raman lines at 1380 and 1444 cm^{-1}, and a very strong and broad Raman band at 1506 cm^{-1}. C(sp^2)−C(Cl) stretching modes have a very low intensity and appear as very weak IR lines at 1114, 1149, and 1168 cm^{-1} and as a medium Raman band at 1138 cm^{-1}.

Absorption and Emission Spectra. $C_{60}Cl_{30}$ has a rather low solubility in common organic solvents (ca. 0.1 mg·mL^{-1} in toluene, much lower in CH_2Cl_2 and *n*-hexane), and its solutions have a dark-yellow color, unlike other, emerald-green, [18]-trannulenes. Figure 3 shows room-temperature absorption spectra measured in *n*-hexane and toluene. Similar spectra with 1−5 nm variation of the band positions were recorded in dichloromethane and *o*-dichlorobenzene as well as in the solid phase (either thin film of pure $C_{60}Cl_{30}$ or KBr pellet). In toluene, the lowest energy absorption of $C_{60}Cl_{30}$ in the visible range occurs at 531 nm (2.335 eV, ϵ = 12 990 L·mol^{-1}·cm^{-1}), and then it is followed by the band at 507 nm (2.445 eV, ϵ = 16 450) with the shoulder at 511 nm (2.426 eV, $\epsilon \sim$ 11 000) and a strong band at 464 nm (2.672 eV, ϵ = 21 600) with the broad "tail" to higher energy and absorption maxima at 449 nm (sh, ϵ = 11 720), 435 (ϵ = 11 180), 423 nm (ϵ = 12 550), 404 nm (ϵ = 13 240), and 380 nm (ϵ = 7710). In the UV range, a strong band at 195 nm ($\epsilon \sim$ 80 000) with unresolved shoulders at 228, 255, and 275 nm was observed in *n*-hexane solution. A series of the low intensity absorptions (ϵ < 650) can be detected in the 570−770 nm range; the most intense ones occur at 711 nm (1.744 eV, ϵ = 615), 736 nm (1.684 eV, ϵ = 252), and 758 nm (1.636 eV, ϵ = 91). Low-temperature spectra of the frozen toluene solutions (Figure 4) showed significant narrowing of the absorption bands and rich vibrational structure in the visible range, and more than 20 bands totally can be distinguished between 350 and 550 nm. In comparison to other [18]-trannulenes, $C_{60}Cl_{30}$ absorptions in the visible range are much more narrow and are considerably blue-shifted (viz., lowest energy reported absorptions occur at 666 and 612 nm in $C_{60}F_{15}R_3$[4,5] and at 850 and 760 nm in $C_{60}R_6$[6]). The extinction coefficient of $C_{60}Cl_{30}$ absorption band at 531 nm (ϵ = 12 990) is close to the value reported for $C_{60}R_6$ absorption at 850 nm (ϵ = 12 755).[6]

Fluorescence emission spectrum of $C_{60}Cl_{30}$ in toluene exhibits two groups of bands with ca. 1:10 intensity ratio. Low intensity features are observed around 1.55−1.77 eV (700−800 nm,

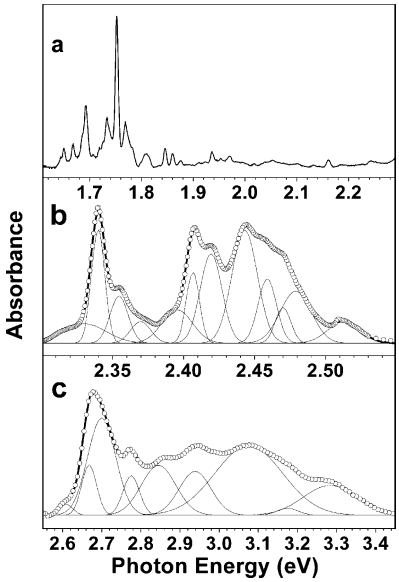

Figure 4. Absorption spectra of $C_{60}Cl_{30}$ at $T \sim 100$ K: (a) in crystalline toluene, (b, c) in glassy toluene. Line shape analysis is shown for b and c; see Supporting Information for details.

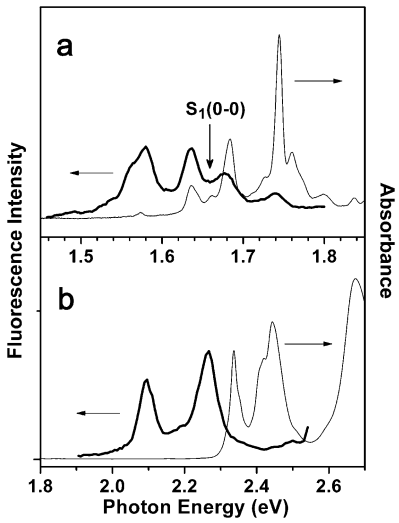

Figure 5. Fluorescence (thick lines) and corresponding absorption (thin lines) spectra of $C_{60}Cl_{30}$. Intensity scale in a is 10 times smaller than in b. Fluorescence excitation wavelength is matched to the absorption at 2.68 eV. Fluorescence intensity in b is matched to the absorption band at 2.337 eV; see text for details of an alternative assignment.

Figure 5a). Because of the very low emission intensity, we had to suppress the spectral resolution to achieve an acceptable signal-to-noise ratio, so intensity and band positions in the emission spectrum are only approximate. Keeping these uncertainties in mind, one can see that the fluorescence spectrum in this range is in reasonable agreement with the mirror-imaged absorption spectrum. From these data, the lowest singlet excited state of $C_{60}Cl_{30}$ can be estimated as 1.66−1.67 eV. 0−0 transition appears to be dipole forbidden and probably corresponds to the weak feature at 1.661 eV (746 nm) at room temperature and 1.668 eV in the crystalline toluene at 100 K. All other bands observed in absorption and emission spectra are due to vibronically activated transitions. Two vibrational modes, ca. 190 and 700 cm^{-1}, exhibit high vibronic activity, and each mode appears both in Stokes and anti-Stokes regimes.

Fluorescence spectrum at higher energy is more peculiar. Two bands are observed at 2.095 eV (592 nm) and 2.266 eV (547 nm), and at first sight, this pattern violates mirror-image absorption spectrum in this range (Figure 5b). Our initial intention was to suppose that the band at 2.265 eV is the emission counterpart of the absorption maximum at 2.337 eV (531 nm), and both correspond to 0−0 components of $S_0 \leftrightarrow S_2$ transitions, which implies a rather high Stokes shift of 570 cm^{-1}. The second emission peak, at 2.095 eV, could be assigned to the vibronic replica of the (0−0) $S_2 \rightarrow S_0$ transition induced by the vibrational mode with ca. 1400 cm^{-1} frequency. However, an analogous vibronic band does not appear in the absorption spectrum. Instead, a group of absorption bands is observed 600−1000 cm^{-1} higher in energy than the proposed (0−0) $S_2 \leftarrow S_0$ absorption, but such a strong softening of the vibrational mode in the singlet excited state is hardly possible. An alternative interpretation may be in the assumption that the band at 2.337 eV corresponds to $S_3 \leftarrow S_0$ transition, while $S_2 \leftarrow S_0$ transition occurs ca. 100 cm^{-1} lower. It appears as a poorly resolved shoulder in the red-side tail of the 2.337 eV absorption band at room temperature but can be clearly distinguished as a peak at 2.330 eV upon cooling the toluene solution to the liquid nitrogen temperature. In this case, the peak at 2.513 eV in the low-temperature absorption spectrum can be assigned to the vibronic transition ($\Delta = 1470$ cm^{-1}), corresponding to the peak at 2.095 eV in the emission spectrum.

Strong similarities can be found between our spectroscopic data for $C_{60}Cl_{30}$ and electron and vibrational spectra of the compound with the brutto composition "$C_{60}Cl_{24}$", synthesized by direct chlorination of C_{60} at 600 K.[16−18] First, absorption spectra of "$C_{60}Cl_{24}$"[16−18] are very similar to those shown in Figures 3 and 4 in this work, including the system of weak bands in the 1.5−1.8 eV range. Second, most of the Raman lines of "$C_{60}Cl_{24}$" registered in ref 16 at 135, 269, 301, 570, 616, 697, 752, 831, 1385, and 1508 cm^{-1} coincide within 1−2 cm^{-1} with the Raman lines of $C_{60}Cl_{30}$ measured in this work (Table 1). Finally, Raman spectra of "$C_{60}Cl_{24}$" could be observed only in the resonant conditions when excitation laser lines were close to the absorption band at 2.33 eV.[16] Besides strong resonant enhancement, authors of that study observed repetition of the vibrational and luminescence spectra shifted by the frequency of the Raman-active phonon at 1508 cm^{-1}, which is in line with our fluorescence spectra. Interpretation of the spectra in refs 16−18 was based on the assumption that "$C_{60}Cl_{24}$" was a single compound; however, it has never been proved. The only individual compound with $C_{60}Cl_{24}$ composition reported to date has T_h molecular symmetry,[14] and its absorption spectrum predicted in ref 17 cannot account for experimental absorptions of "$C_{60}Cl_{24}$". Spectroscopic characterization of $C_{60}Cl_{30}$, which is undoubtedly a single compound, enables us to conclude that direct chlorination of C_{60} led to a mixture of products (rather than an individual $C_{60}Cl_{24}$), which contained $C_{60}Cl_{30}$ among the other components. From this fact, we can benefit precise determination of the vibrational mode coupled to the $S_{3(2)} \rightarrow S_0$ emission, which is not possible with our fluorescence data. Raman-active phonon at 1508 cm^{-1} in ref 16 corresponds to the strong Raman line at 1506 cm^{-1} observed in this work and assigned to E_g-symmetric stretching vibration of the trannulene belt.

Frontier Orbital Analysis. To rationalize experimentally observed absorption and emission spectra, we have performed a series of quantum-chemical calculations of the electronic structure and excitations in $C_{60}Cl_{30}$, $C_{60}F_{15}H_3$, and $C_{60}H_6$ molecules. Two molecules were also considered as model compounds: C_{60}, whose electronic structure is well-known, and hypothetical [18]trannulene, $C_{18}H_{18}$. For the sake of conven-

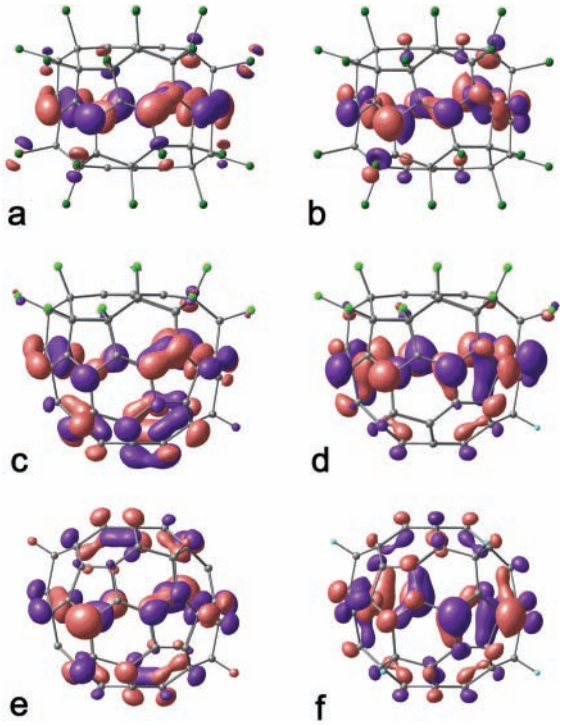

Figure 6. Spatial distribution of HOMO (a, c, e) and LUMO (b, d, f) in $C_{60}Cl_{30}$, $C_{60}F_{15}H_3$, and $C_{60}H_6$, respectively.

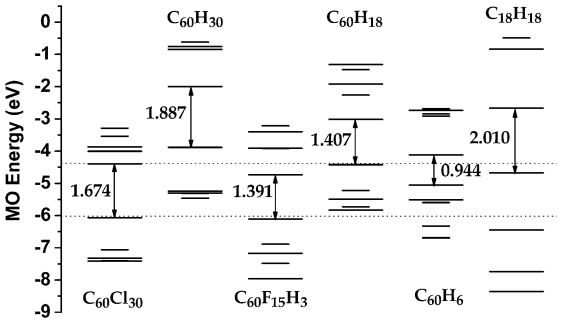

Figure 7. PBE/TZ2P Kohn−Sham MO levels in [18]trannulenes $C_{60}Cl_{30}$, $C_{60}H_{30}$, $C_{60}F_{15}H_3$, $C_{60}H_{18}$, $C_{60}H_6$, and $C_{18}H_{18}$. HOMO−LUMO gaps are denoted by arrows. Dotted lines show HOMO and LUMO levels in C_{60}.

ience, $C_{18}H_{18}$ is treated in D_{3d} point group, though its actual symmetry is D_{9d}.

Figure 6 shows visualization of Kohn−Sham highest occupied and lowest unoccupied molecular orbitals (HOMO and LUMO) in $C_{60}Cl_{30}$, $C_{60}F_{15}H_3$, and $C_{60}H_6$[19] as computed at the PBE/TZ2P level, while Figure 7 depicts electronic energy levels in these molecules. HOMO and LUMO in all [18]trannulenes are 2-fold degenerated. Within D_{3d} molecular symmetry (as in $C_{60}Cl_{30}$ and $C_{60}H_6$), HOMO/LUMO have E_g/E_u symmetry, respectively, while in the framework of C_{3v} group ($C_{60}F_{15}H_3$) both HOMO and LUMO have E symmetry as found earlier by Burley et al.[20] As can be seen from their graphical representations, HOMO and LUMO of $C_{60}Cl_{30}$, $C_{60}F_{15}H_3$, and $C_{60}H_6$ are mostly localized on the trannulene subunits. At the same time, the extent of localization is quite different for these molecules. Quantifying localization degree as a sum of squared coefficients of atomic orbitals in Lowdin orthogonalized MOs for all 18 carbon atoms comprising [18]trannulene subunit, we have 72, 52, and 49% for HOMOs of $C_{60}Cl_{30}$, $C_{60}F_{15}H_3$, and $C_{60}H_6$, respectively; similar values, 75, 54, and 51%, are obtained with the use of Mulliken atomic population analysis. For LUMOs, localization degree on the trannulene moiety is 60% in $C_{60}Cl_{30}$, 72% in $C_{60}F_{15}H_3$, and 51% in $C_{60}H_6$. The trend observed for HOMO correlates with two other tendencies in $C_{60}Cl_{30}$−$C_{60}F_{15}H_3$−$C_{60}H_6$ row, namely, increase of the partial conjugation of [18]-trannulene with the remaining π-system (the absence of adjacent π-subsystems in $C_{60}Cl_{30}$ versus one or two triphenylene subunits in $C_{60}F_{15}H_3$ and $C_{60}H_6$, respectively) and the drastic decrease of the HOMO−LUMO gap (the value for $C_{60}Cl_{30}$ is quite close to that computed for C_{60}). To evaluate whether conjugation of the [18]trannulene with the remaining π-system is the only factor responsible for the changes in the HOMO/LUMO gap or whether the nature and amount of the substituents (viz., Cl or F atoms) are also important, we have performed computations for two hypothetical hydrofullerenes, $C_{60}H_{30}$ and $C_{60}H_{18}$, with the same addition patterns as in $C_{60}Cl_{30}$ and $C_{60}F_{15}R_3$. Both HOMO and LUMO appeared to be dramatically destabilized in the hydrofullerenes (ca. +2.2 eV for $C_{60}H_{30}$ vs $C_{60}Cl_{30}$ and +1.7 eV for $C_{60}H_{18}$ vs $C_{60}F_{15}R_3$), while the HOMO−LUMO gap did not show substantial alteration, being almost the same in $C_{60}H_{18}$ and 0.21 eV higher in $C_{60}H_{30}$. Also, the 1.89 eV gap found for $C_{60}H_{30}$ is rather close to the 2.01 eV value computed for $C_{18}H_{18}$ trannulene (Figure 7). Thus, we conclude that the presence of electron-withdrawing substituents in close proximity of the [18]trannulene moieties results in the overall stabilization of MOs with only secondary influence on the HOMO−LUMO gap. The differences in HOMO−LUMO gaps and corresponding optical properties of the fullerene-based trannulenes mostly result from the interaction of the [18]trannulene moieties with the remaining π-subsystems.

TD-DFT Computations and Assignment of the Electronic Spectra. HOMO→LUMO transitions in [18]trannulenes occur between 2-fold degenerated MOs and should yield three excited states, with either $A_{1u}+A_{2u}+E_u$ (D_{3d}) or A_1+A_2+E (C_{3v}) symmetry types. Deeper insight into the nature and energy of excited states requires theoretical modeling of the electron excitation spectra. Bauernschmitt et al.[21] reported that time-dependent (TD) DFT approach with generalized gradient approximation (GGA) functional BP86 yields good agreement with the absorption spectra of fullerenes. On another hand, Grimme et al.[22,23] have shown that TD-DFT(GGA) approaches may yield significant errors for excitation energies in conjugated systems. These errors most probably originate from the wrong asymptotic behavior of approximate exchange functionals. To avoid misinterpretation which may stem from inadequate use of the computational techniques, a series of computations with gradually increasing exact exchange component (EEX) were performed, namely, using pure GGA PBE functional[12] and hybrid PBE0[24] and HHBLYP[25,26] functionals (25% and 50% of EEX, respectively) as well as pure ab initio CIS and TD-HF (also known as RPA) approximations (100% EEX). Because of the high computational demands, only the lowest excited states could be accessed in this work, and we focus our attention on the low-energy part of the spectra. Computed excitation energies and oscillator strengths are given in Table 2.

Irrespective of the computational method used, the first excited state is predicted to have either A_{1u} or A_2 symmetry in all [18]trannulenes studied, that is, S_1←S_0 transition is dipole forbidden. Thus, we may confirm our experimentally based assignment and propose that low-intensity bands around 1.6−2.2 eV in the absorption and emission spectra of $C_{60}Cl_{30}$ are due to vibronic $S_1(A_{1u})$←S_0 transitions, activated by Herzberg−Teller mechanism through coupling with A_{2g} and E_g vibrational modes and, probably, their Franck−Condon progressions. Very weak bands ($\epsilon \sim 500$) at 1.23 eV (1010 nm) and 1.14 eV (1080

TABLE 2: Selected Excitation Energies (eV) and Oscillator Strengths (in Parentheses for Dipole-Allowed Transitions) of C_{60}, $C_{60}Cl_{30}$, $C_{60}F_{15}H_3$, $C_{60}H_6$, and $C_{18}H_{18}$ Computed at TD-DFT, TD-HF, and CIS Levels of Theory

S_n	PBE[a]	PBE[b]	PBE0	BHHLYP	TD-HF	CIS	exptl
				C_{60}			
1^1G_g	1.658	1.708	2.160	2.466	2.814	3.020	1.93−1.95[c]
1^1F_{1g}	1.700	1.752	2.160	2.547	3.237	3.312	1.93−1.95[c]
1^1F_{2g}	1.719	1.773	2.163	2.492	3.382	3.479	1.93−1.95[c]
1^1F_{1u}	2.777 (0.004)	2.820 (0.005)	3.618 (0.055)	4.319 (0.514)	5.275 (2.031)	5.537 (1.643)	3.04 (0.015)[d]
2^1F_{1u}		3.470 (0.291)	4.046 (0.545)	4.651 (0.486)	6.315 (0.201)	6.329 (0.093)	3.78 (0.370)[d]
				$C_{60}Cl_{30}$			
1^1A_{1u}	1.699	1.728	1.904	1.851	1.058	2.029	1.66−1.67
1^1A_{2u}	1.825 (0.024)	1.864 (0.027)	2.208 (0.079)	2.269 (0.137)	1.696 (0.259)	2.398 (0.203)	2.33−2.34
2^1A_{2u}		2.203 (0.026)	2.786 (0.010)	3.399 (0.004)	4.564 (0.001)	4.609 (0.001)	2.4−2.5
1^1E_u	1.931 (0.048)	1.974 (0.050)	2.560 (0.310)	2.931 (0.932)	3.302 (1.486)	3.799 (2.727)	2.33−2.34
2^1E_u		2.605 (0.714)	3.015 (0.803)	3.500 (0.410)	4.637 (0.187)	4.700 (0.598)	2.68
				$C_{60}F_{15}H_3$			
1^1A_2	1.401	1.422	1.579	1.594	1.045	1.801	
1^1A_1	1.591 (0.026)	1.625 (0.027)	1.893 (0.053)	2.020 (0.092)	1.673 (0.183)	2.262 (0.190)	1.86[e]
2^1A_1	2.182 (0.004)	2.271 (0.004)	2.871 (0.010)	3.235 (0.005)	3.810 (0.000)	3.971 (0.000)	
1^1E	1.636 (0.050)	1.671 (0.052)	1.958 (0.099)	2.209 (0.166)	2.624 (0.169)	2.846 (0.237)	1.86[e]
2^1E	2.188 (0.007)	2.276 (0.008)	2.781 (0.002)	3.192 (0.003)	3.865 (0.002)	4.011 (0.002)	
				$C_{60}H_6$			
1^1A_{1u}	0.948	0.983	1.112	1.150	0.724	1.359	
1^1A_{2u}	1.126 (0.024)	1.176 (0.025)	1.438 (0.050)	1.608 (0.089)	1.432 (0.190)	1.924 (0.227)	1.47[f]
2^1A_{2u}	2.432 (0.006)	2.477 (0.007)	2.954 (0.012)	3.287 (0.012)	3.754 (0.007)	3.954 (0.004)	
1^1E_u	1.114 (0.024)	1.162 (0.026)	1.391 (0.048)	1.612 (0.079)	1.979 (0.079)	2.153 (0.131)	1.47[f]
2^1E_u	2.261 (0.000)	2.333 (0.000)	2.907 (0.000)	3.395 (0.011)	4.407 (0.023)	4.201 (0.018)	
				$C_{18}H_{18}$			
1^1A_{1u}	2.047	2.076	2.111	1.947	0.864	2.063	
1^1A_{2u}	2.275 (0.008)	2.328 (0.009)	2.491 (0.020)	2.440 (0.037)	1.722 (0.085)	2.479 (0.069)	
2^1A_{2u}	4.760 (0.000)	5.023 (0.000)	5.986 (0.000)	6.789 (0.000)	7.491 (0.000)	7.903 (0.000)	
1^1E_u	3.577 (3.326)	3.699 (3.220)	3.813 (3.492)	3.895 (3.710)	4.082 (4.158)	4.947 (9.211)	
2^1E_u	4.239 (0.000)	4.665 (0.000)	5.409 (0.000)	5.895 (0.000)	6.869 (0.000)	6.971 (0.000)	

[a] RI-DFT calculations with TZ2P basis set, PRIRODA package.[10,11] [b] 6-31G* basis set, conventional evaluation of Coulomb and exchange terms, PC GAMESS package.[13] [c] Reference 27. [d] Reference 28. [e] References 4 and 5. [f] Reference 6.

nm) can be distinguished in the absorption spectra of $C_{60}R_6$[6] and may also originate from the vibronically activated $S_1 \leftarrow S_0$ transition.

While all computational methods agree qualitatively for the first excited state, quantitative agreement is by no means achieved. For C_{60}, the increase of EEX leads to the gradual increase of the excitation energies. Inclusion of 25% EEX in PBE0 method increases the lowest excitation energies by ca. 0.4 eV over PBE. TD-PBE excitation energy is ca. 0.25 eV underestimated, while TD-PBE0 is 0.20 eV higher than the experimental values. Further increase of the EEX leads to significant overestimation of the excitation energies reaching errors of more than 1 eV for Hartree−Fock based TDHF and CIS methods. The situation is different for [18]trannulenes. All TD-DFT values are somewhat overestimated. Among them, TD-PBE provides the best match to the experimental $S_1 \leftarrow S_0$ excitation energy in $C_{60}Cl_{30}$, but PBE/TZ2P HOMO−LUMO gap (Figure 7) is an even better approximation for the experimental value. For the hybrid functionals, S_1 energies are 0.15−0.20 eV higher than TD-PBE ones, but TD-PBE0 and TD-BHHLYP values are almost the same (for S_1-S_3 states of C_{60}, TD-BHHLYP energies were 0.3−0.4 eV higher than TD-PBE0). Furthermore, the excitation energy drops dramatically when EEX is increased to 100% in TD-HF method, while CIS values remain higher than TD-DFT ones.

Results of the calculations become more diverged as higher energy dipole-allowed excitations are considered. First, we check validity of the computational approaches by their predictions of two lowest dipole-allowed transitions in C_{60} at 3.04 and 3.80 eV.[21,28] TD-PBE values exhibit the best fit to the experimental data, both in excitation energies and in oscillator strengths. The only imperfection is the systematic 0.2−0.3 eV underestimation of the excitation energies, which is also consistent with TD-BP86 data.[21] Similar accuracy is achieved within TD-PBE0, the energies and intensities being somewhat overestimated. Further increase of EEX leads both to substantial overestimation of the energies and incorrect oscillator strengths, the latter expressing itself in the interchange of the relative intensities between the first and the second transitions and overall increase of the intensities. Thus, reliable predictions of excitation spectra in C_{60} may be achieved only with the moderate fraction of the EEX term.

The influence of EEX fraction on predicted excitation energies of $C_{18}H_{18}$ is quite different than for C_{60}. TD-PBE0, TD-BHHLYP, and TD-HF excitation energies and oscillator strengths for 1^1A_{2u} and 1^1E_u states are almost the same and are slightly higher than TD-PBE ones. Similarly to the 1^1A_{1u} state, there is a significant difference between CIS and TD-HF excitation energies, while in the C_{60} case the difference is always less than 0.2 eV. Other specific features of $C_{18}H_{18}$ are very high intensity predicted for $1^1E_u \leftarrow S_0$ transition and 1.3−1.4 eV splitting between 1^1A_{2u} and 1^1E_u states, though both are described as HOMO→LUMO excitations.

Fullerene-based [18]trannulenes are different both from C_{60} and $C_{18}H_{18}$ but at the same time inherit some properties from both predecessors. On one hand, the 1^1A_{2u} (1^1A_1) state is markedly similar to that in $C_{18}H_{18}$: TD-PBE0 and TD-BHHLYP energies are similar and slightly higher than TD-PBE ones, while TD-HF is significantly lower. Oscillator strength for this transition is also very close to that predicted for $C_{18}H_{18}$. On the other hand, the splitting between 1^1A_{2u} and 1^1E_u states is only marginal within TD-DFT approaches, and $1^1E_u \leftarrow S_0$ transition

intensity is much lower than in $C_{18}H_{18}$ at TD-PBE and TD-PBE0 levels. Similar to transitions in C_{60}, increase of the EEX fraction results in the growths of the energy and oscillator strength of $1^1E_u \leftarrow S_0$ transition without any peculiarity at the TD-HF level. This indicates that electron excitations in $C_{60}R_6$, $C_{60}F_{15}R_3$, and even $C_{60}Cl_{30}$ cannot be modeled by excitations in the trannulene unit alone and are strongly influenced by the interactions with the remaining parts of the molecules.

Assignment of the low-energy part of $C_{60}F_{15}R_3$ and $C_{60}R_6$ absorption spectra is straightforward. All TD-DFT methods predict that $1^1A_{2u}(1^1A_1)$ and $1^1E_u(1^1E)$ states are quasi-degenerated, their energies are quite close to the experimental features at 1.47 eV ($C_{60}R_6$)[6] and 1.86 eV ($C_{60}F_{15}R_3$),[4,5] and no other dipole-allowed transitions are expected in these ranges. Thus, we propose that the low-energy components of characteristic double peaks in the absorption spectra of $C_{60}F_{15}R_3$ and $C_{60}R_6$ are due to $1^1E_u(1^1E) \leftarrow S_0$ and $1^1A_{2u}(1^1A_1) \leftarrow S_0$ transitions. The second feature observed in the spectra of both compounds is shifted by ca. 1400 cm^{-1} to higher energy and most likely corresponds to the vibronically induced transitions similar to that in $C_{60}Cl_{30}$ (see Figure 5b and discussion below). This assumption is also confirmed by the double peak observed in the fluorescence spectrum of $C_{60}F_{15}R_3$.[9]

Assignment of $C_{60}Cl_{30}$ electronic spectra is complicated by uncertainties in the interpretation of the fluorescence spectra and predictions of two more allowed transitions in the close proximity of 1^1A_{2u} and 1^1E_u states. The key to assignment of the lowest dipole-allowed transition is the fact that it is coupled to the nontotally symmetric E_g vibrational mode (see discussion of the fluorescence spectrum above and its relations to spectroscopic data on $C_{60}Cl_{24}$[16]). Thus, it cannot be a transition involving a nondegenerated 1^1A_{2u} state, and we conclude that $1^1E_u \leftarrow S_0$ transition occurs at 2.33 eV. On the other hand, all computational methods employed predict that 1^1A_{2u} state has lower energy than 1^1E_u, and in analogy with $C_{60}F_{15}R_3$ and $C_{60}R_6$, we propose that 1^1A_{2u} and 1^1E_u states are quasi-degenerated. Total oscillator strength for the absorption band at 2.33 eV is 0.03 which agrees with the oscillator strengths of $1^1E_u \leftarrow S_0$ and $1^1A_{2u} \leftarrow S_0$ transitions predicted at the TD-PBE and TD-PBE0 levels. Assignment of $2^1E_u \leftarrow S_0$ transition is facilitated by its high predicted oscillator strengths. Since higher energy dipole-allowed transitions have much lower predicted intensities, we may safely assign the strongest absorption in the visible range at 2.67 eV to the $2^1E_u \leftarrow S_0$ transition. Finally, the energy of 2^1A_{2u} state is predicted to be lower than that of 2^1E_u state, while oscillator strength of $2^1A_{2u} \leftarrow S_0$ excitation is similar to that of $1^1A_{2u} \leftarrow S_0$ and $2^1E_u \leftarrow S_0$. Hence, we tentatively propose that $2^1A_{2u} \leftarrow S_0$ transition corresponds to one of the absorption bands around 2.4−2.5 eV.

Additional low-energy transitions in $C_{60}Cl_{30}$ are due to the LUMO(+1) which also has E_u symmetry and is predicted to be only 0.39 eV above the LUMO (Figure 7). Depending on the EEX fraction, LUMO(+1) has different spatial distributions: at the PBE level, it is equally localized on the trannulene moiety and benzene rings; at BHHLYP and HF levels, the contribution from benzene rings is dominating; and PBE0 functional yields intermediate distribution. These differences are inherited in the configurations describing excited states. Thus, both $1^1E_u \leftarrow S_0$ and $2^1E_u \leftarrow S_0$ excitations have equal contributions from HOMO→LUMO and HOMO→LUMO(+1) at the TD-PBE level, TD-PBE0 predicts 65% HOMO→LUMO and 35% HOMO→LUMO(+1) contributions to $1^1E_u \leftarrow S_0$ and vice versa for $2^1E_u \leftarrow S_0$, while BHHLYP, TD-HF, and CIS predict 100% HOMO→LUMO and 100% HOMO→LUMO(+1) for $1^1E_u \leftarrow S_0$ and $2^1E_u \leftarrow S_0$, respectively. Whatever is true, it is clear that excited states involving HOMO→LUMO(+1) configurations should have significant ionic components and thus exhibit difficulties for TD-DFT.[22,23] A more reliable assignment requires modeling of the vibronic structure for these states which is underway in our group.

Conclusions

IR and Raman spectroscopic characterization of $C_{60}Cl_{30}$ is provided and the spectra are assigned with the use of DFT vibrational computations. It is found that HOMO−LUMO gap and electron excitation spectra of [18]trannulenes are strongly influenced by the interactions of trannulene moieties with the remaining π-subsystems of the molecules. Fluorescence of $C_{60}Cl_{30}$ proceeds from two excited states, and like absorption spectra exhibit rich vibrational structure. With the help of TD-DFT computations, we have shown that all [18]trannulenes have dipole-forbidden lowest excited state, which in the case of $C_{60}Cl_{30}$ can be detected in the absorption and emission spectra because of the weak vibronic transitions induced by the Herzberg−Teller mechanism. Characteristic absorption bands observed in the spectra of [18]trannulenes are assigned to quasi-degenerated dipole-allowed $S_2,S_3 \leftarrow S_0$ transitions with leading contributions from HOMO−LUMO excitations.

Acknowledgment. We acknowledge Research Computing Center of the Moscow State University for computer time, Analytik Jena (Germany) for providing us with Specord-200, and Russian Foundation for Basic Research for financial support (grant 05-03-04006). We thank Mr. V. Korepanov for assistance in fluorescence measurements.

Supporting Information Available: Details of vibrational calculations, complete list of vibrational frequencies and PED normal-mode analysis, line-shape analysis of the low-temperature absorption spectrum, and DFT-computed HOMO and LUMO energies in $C_{60}F_{15}R_3$ and $C_{60}R_6$ with different R. This material is available free of charge via the Internet at http://pubs.acs.org.

References and Notes

(1) Troyanov, S. I.; Kemnitz, E. *Eur. J. Org. Chem.* **2005**, 4951.

(2) Troyanov, S. I.; Shustova, N. B.; Popov, A. A.; Sidorov, L. N. *Russ. Chem. Bull., Int. Ed.* **2005**, *7*, 1656 (translated from *Izvestiya Akad. Nauk, Ser. Khim.* **2005**, *7*, 1608).

(3) Troshin, P. A.; Lyubovskaya, R. N.; Ioffe, I. N.; Shustova, N. B.; Kemnitz, E.; Troyanov, S. I. *Angew. Chem., Int. Ed.* **2005**, *44*, 234.

(4) Wei, X.-W.; Darwish, A. D.; Boltalina, O. V.; Hitchcock, P. B.; Street, J. M.; Taylor, R. *Angew. Chem., Int. Ed.* **2001**, *40*, 2989.

(5) Burley, G. A.; Avent, A. G.; Gol'dt, I. V.; Hitchcock, P. B.; Al-Matar, H.; Paolucci, D.; Paolucci, F.; Fowler, P. W.; Soncini, A.; Street, J. M.; Taylor, R. *Org. Biomol. Chem.* **2004**, *2*, 319.

(6) Canteenwala, T.; Padmawar, P. A.; Chiang, L. Y. *J. Am. Chem. Soc.* **2005**, *127*, 26.

(7) Burley, G. A. *Angew. Chem., Int. Ed.* **2005**, *44*, 376.

(8) Burley, G. A.; Avent, A. G.; Boltalina, O. V.; Gol'dt, I. V.; Guldi, D. M.; Marcaccio, M.; Paolucci, F.; Paolucci, D.; Taylor, R. *Chem. Commun.* **2003**, 148.

(9) Guldi, D. M.; Marcaccio, M.; Paolucci, F.; Paolucci, D.; Ramey, J.; Taylor, R.; Burley, G. A. *J. Phys. Chem. A* **2005**, *109*, 9723.

(10) Laikov, D. N. *Chem. Phys. Lett.* **1997**, *281*, 151.

(11) Laikov, D. N.; Ustynyuk, Y. A. *Russ. Chem. Bull.* **2005**, *54*, 820.

(12) Perdew, J. P.; Burke, K.; Ernzerhof, M. *Phys. Rev. Lett.* **1996**, *77*, 3865.

(13) Granovsky, A. A. PC GAMESS URL: http://classic.chem.msu.su/gran/gamess/index.html, 2006.

(14) Shustova, N. B.; Popov, A. A.; Sidorov, L. N.; Turnbull, A. P.; Kemnitz, E.; Troyanov, S. I. *Chem. Commun.* **2005**, 1411.

(15) Kuvychko, I. V.; Streletskii, A. V.; Popov, A. A.; Kotsiris, S. G.; Drewello, T.; Strauss, S. H.; Boltalina, O. V. *Chem. Eur. J.* **2005**, *11*, 5426.

(16) Limonov, M. F.; Kitaev, Yu. E.; Chugreev, A. V.; Smirnov, V. P.; Grushko, Yu. S.; Kolesnik, S. G.; Kolesnik, S. N. *Phys. Rev. B* **1998**, *57*, 7586.

(17) Coheur, P.-F.; Lievin, J.; Colin, R.; Razbirin, B. *J. Chem. Phys.* **2003**, *118*, 550.

(18) Rasbirin, B. S.; Starukhin, A. N.; Chugreev, A. V.; Smirnov, V. P.; Grushko, Yu. S.; Kolesnik, S. G.; Coheur, P.-F.; Lievin, J.; Colin, R. *Phys. Solid State* **2002**, *44*, 2204.

(19) Testing calculation has shown that substitution of malonate groups by H atoms do not impose significant changes in the structure of frontier MOs in $C_{60}F_{15}R_3$ and $C_{60}R_6$. A series of calculations were also performed with R = F, CH_3, CH_2F, CHF_2, or CF_3; while the energies of the MOs were significantly altered by the nature of R, HOMO−LUMO gap was almost constant. See Supporting Information for details.

(20) Burley, G. A.; Fowler, P. W.; Soncini, A.; Sandall, J. P. B.; Taylor, R. *Chem. Commun.* **2003**, 3042.

(21) Bauernschmitt, R.; Ahlrichs, R.; Hennrich, F. H.; Kappes, M. M. *J. Am. Chem. Soc.* **1998**, *120*, 5052.

(22) Grimme, S.; Parac, M. *ChemPhysChem.* **2003**, *4*, 292.

(23) Parac, M.; Grimme, S. *Chem. Phys.* **2003**, *292*, 11.

(24) Perdew, J. P.; Ernzerhof, M.; Burke, K. *J. Chem. Phys.* **1996**, *105*, 9982.

(25) Becke, A. D. *Phys. Rev. A* **1988**, *38*, 3098.

(26) Lee, C.; Yang, W.; Parr, R. G. *Phys. Rev. B* **1988**, *37*, 785.

(27) Orlandi, G.; Negri, F. *Photochem. Photobiol. Sci.* **2002**, *1*, 289, and references therein.

(28) Leach, S.; Vervloet, M.; Despres, A.; Breheret, E.; Hare, J. P.; Dennis, T. J.; Kroto, H. W.; Taylor, R.; Walton, D. R. M. *Chem. Phys.* **1992**, *160*, 451.